JOURNAL OF AIRCRAFT
Vol. 31, No. 3, May–June 1994

Design of Optimized Airfoils in Subcritical Flow

J. Olejniczak* and A. S. Lyrintzis†
University of Minnesota, Minneapolis, Minnesota 55455

An airfoil design method based on optimization procedures in computational aerodynamics is presented. This article extends the method to include subcritical compressible flow and a modified Stratford recovery distribution to alleviate the hard stall that is typical of Stratford-type airfoils. A procedure for optimizing the drag is also presented based on the Squire-Young drag formula. The performance characteristics of this airfoil are then tested with a compressible panel method and boundary-layer solver. The procedures for both incompressible and compressible flow have generated airfoils which generate more lift and less drag than other comparable airfoils. High-lift airfoils which display a smooth stall region have also been developed which hold promise for general aviation use. In addition, these airfoils offer the potential of improved performance in applications such as high-endurance aircraft, propellers, fans, and windmill blades where high lift-to-drag ratios are desired. A specific example of an airfoil designed for a wind turbine is presented and compared to an existing airfoil.

Nomenclature

$a(\zeta)$ = slope of modified Stratford distribution
C_D = drag coefficient
C_L = lift coefficient
C_P = pressure coefficient
$\bar{C}_P$ = Stratford pressure coefficient
$\bar{C}_{P_M}$ = modified Stratford pressure coefficient
L/D = airfoil lift-to-drag ratio
M = Mach number
PR = pressure recovery factor
Re = Reynolds number
s = arc length along airfoil measured counterclockwise from trailing edge
V = velocity on the airfoil surface
XT = trailing-edge location of airfoil
x_0 = distance of constant pressure region on upper airfoil surface
α = angle of attack
β = leading-edge slope of velocity distribution
γ = ratio of specific heats
θ = boundary-layer momentum thickness
μ = parameter in velocity recovery distribution

Subscripts

e = boundary-layer edge conditions
t = boundary-layer transition point on airfoil surface
te = trailing edge
0 = conditions when $C_P = C_{P\text{minn}}$ on airfoil upper surface
1 = point on airfoil corresponding to beginning of rooftop velocity region
2 = point on airfoil corresponding to beginning of lower surface velocity distribution
3 = trailing edge of airfoil
∞ = freestream conditions

Received Nov. 28, 1992; presented as Paper 93-0532 at the AIAA 31st Aerospace Sciences Meeting, Reno, NV, Jan. 11–14, 1993; revision received April 25, 1993; accepted for publication July 21, 1993.

*Undergraduate Student, Department of Aerospace Engineering and Mechanics.
†Assistant Professor, Department of Aerospace Engineering and Mechanics. Member AIAA.

I. Introduction

THE problem of optimizing an airfoil for maximum lift was studied by Smith[1] and Liebeck[2–4] in the early seventies. They considered a single-element airfoil in incompressible flow and found analytic expressions for the optimum velocity distribution. This distribution was then modified to ensure a practical airfoil shape, and that shape was then found using a conformal mapping-based inverse scheme. The resulting airfoil can then be tested with panel methods and boundary-layer solvers to determine if the airfoil is really an optimum design.

Since that time much progress has been made and the method has been extended by other investigators such as Lyrintzis et al.,[5] Narramore et al.,[6] and Volpe.[7] Lyrintzis and Farmer[8] considered the nonlinear method developed by Liebeck using the distance along the airfoil as the independent variable. The airfoil shape is then found using an inverse design method developed by Strand.[9] Airfoils were generated with higher lift-to-drag ratios than conventional airfoils considering only incompressible flow. These optimized airfoils have since been further modified by improving the lower airfoil surface and leading edge.

In this article the method is extended to subcritical compressible flow and a modified Stratford pressure recovery region is developed to lessen the hard stall characteristics of the previous high-lift airfoils. In addition, a preliminary investigation is made of optimizing airfoils for minimum drag using an analytical expression for drag based on the potential velocity. Airfoils can also be optimized for a given thickness, which is useful when structural considerations impose constraints on the final airfoil shape. An example design using these methods is presented of an airfoil developed for a windmill blade and compared to an airfoil developed by Tangler.[10] A vortex-based panel method and an integral boundary-layer solver developed by Drela and Giles[11] is used for calculation of lift and drag coefficients plus prediction of boundary-layer behavior and separation. The Von Karmen-Tsien approximation is used to account for compressibility in the panel method, whereas the boundary-layer solver is a fully compressible method.

II. Maximum Lift Airfoils Using Liebeck's Method

The approach to solving the maximum lift design problem is to specify an optimum velocity distribution and then calculate the corresponding airfoil shape. The details of this method are given by Lyrintzis and Farmer,[8] however, a brief summary is included here for completeness.

A nonlinear theory was developed and eventually solved by Liebeck.[4] He considered a calculus of variations problem to maximize the lift subject to the constraints of a single-element airfoil in incompressible flow. Liebeck assumed that the upper surface velocity distribution consisted of an arbitrary acceleration region from the leading-edge stagnation point to a maximum velocity followed by a Stratford[12] pressure recovery region to the trailing-edge velocity.

The Stratford distribution is an analytical expression for the slope of a pressure recovery region based on a zero skin friction criterion throughout the region. It is believed to be ideal for developing high-lift airfoils as Smith[1] showed that the Stratford distribution provides the path of least resistance connecting two pressure points, and therefore recovers a maximum pressure difference in a given distance or a given pressure difference in the shortest possible distance.

The general solution to this problem was found to be flat rooftop region of constant velocity followed by the Stratford pressure recovery region. Strand's[9] conformal mapping procedure is then used to find the shape of the optimized airfoil. For Strand's method the initial input lower surface velocity distribution is modified in a least squares sense to ensure that Lighthill's[13] conditions on the velocity are met to ensure a closed airfoil. At the same time the lower surface velocity distribution is subject to the constraint of continually accelerating flow in order to minimize the drag in the sense of assuring a favorable pressure gradient. It should be noted that the modified velocity distribution can have some waviness if a large modification is needed. Thus, the modified velocity distribution is made smooth and is given as a new input velocity. This procedure results in smooth velocities after 1–2 iterations.

Before any results are presented an explanation of the notation used in this study is in order. Optimized airfoils developed using the OPTIMUM code, a computer program developed to determine the optimum velocity distribution and calculate the inverse airfoil shape, are denoted in the following manner: OPT(M/D).XXXY.ZZ.WW. In this notation the optional M indicates that the lower surface of the airfoil was modified from previous results, while the optional D indicates the airfoil was optimized for minimum drag. XXX then represents either LAM or TUR for laminar or turbulent flow, Y is the Reynolds number in millions, ZZ is the Mach number in hundredths, and WW is the pressure recovery factor *PR*.

Figure 1 shows the original OPT.TUR3.00.00 airfoil,[8] which has a maximum thickness of 12.4%. The large camber near the leading edge and general humpbacked shape are characteristic of high-lift airfoils and are characteristic of those developed by Liebeck.[4] However, the hook nose on the lower surface near the leading edge of OPT.TUR3.00.00 causes a laminar separation bubble to appear. This leads to poor performance at low angles of attack. This undesirable characteristic is removed by altering the lower surface velocity distribution input into the inverse design code. The initial slope of the lower surface velocity distribution is reduced and the form of the remaining distribution is made to better match this slope. This new airfoil, OPTM.TUR3.00.00, is also shown in Fig. 1.

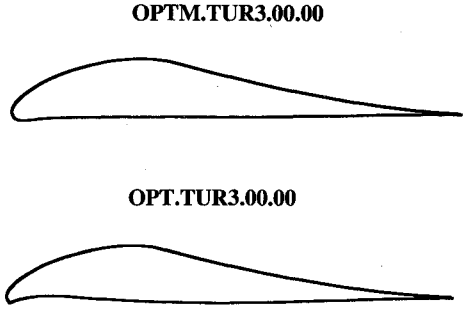

Fig. 1 Comparison of optimized airfoils with and without lower surface modifications.

As a first test of the inverse method used in OPTIMUM, the pressure distribution for the OPTM.TUR3.00.00 airfoil was calculated using the Drela analysis code.[11] Figure 2 shows both the inviscid and viscous pressure distributions for the OPTM.TUR3.00.00 airfoil, as well as the pressure distribution input into the inverse method as generated by OPTIMUM. The resulting distributions are largely as expected. The leading-edge constant slope regions, the flat rooftop region, and the Stratford recovery region can all be seen. The small spike in both pressure distributions at the beginning of the flat rooftop is thought to be caused by the sudden deceleration of the flow as it reaches the rooftop. Physically, the flow overshoots the rooftop velocity, but then settles back to the required value. A possible improvement in these optimized airfoils would be to alter the constant slope region so that this abrupt deceleration could be smoothed.

The lift-to-drag ratios of these two optimized airfoils are compared to results for a NACA 64-(11)12 airfoil at a Reynolds number of 3×10^6 in Fig. 3; Drela's code is used for the evaluation of lift and drag. The NACA 64-(11)12 was chosen because it has a similar thickness distribution as the OPT.TUR3.00.00 airfoil (12% compared to 12.4%), similar $C_{l_o}(0.4)$ and camber. NACA 64-(11)12 with mean line $a = 0.3$ is designed with the same amount of camber and the same length for a flat rooftop as the optimized airfoil, so that the main factor of comparison is the pressure recovery region. Near $\alpha = 9.5$ deg, the optimized airfoil design angle, defined as the angle of attack where the airfoil will have an upper

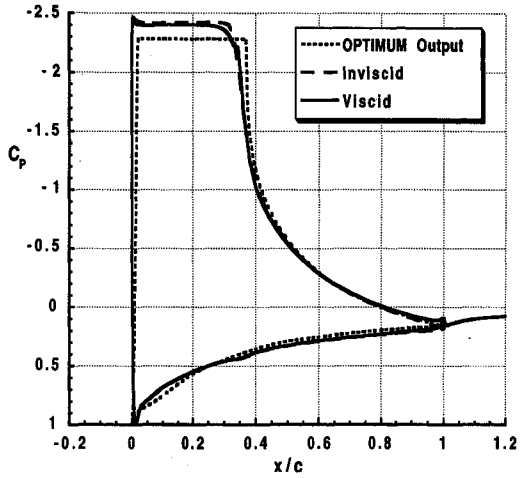

Fig. 2 Velocity distributions calculated by the Drela code as compared to the target velocity distribution.

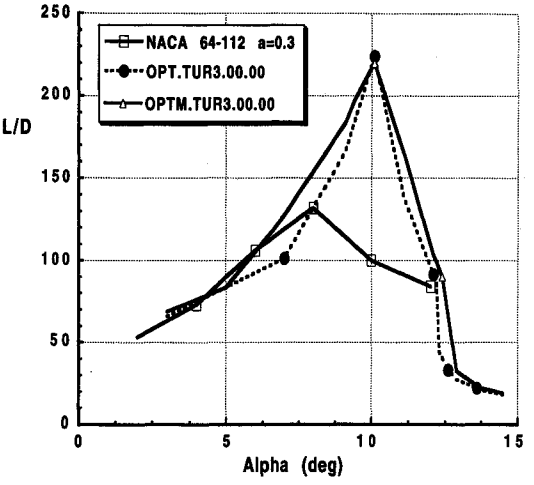

Fig. 3 Lift-to-drag ratios of OPTIMUM airfoils compared to a similar NACA airfoil.

surface pressure distribution consisting of a flat rooftop followed by the Stratford recovery region, the optimized airfoils produce much higher lift-to-drag ratios than the NACA airfoil. Above and below the design angle it can be seen that the OPTM.TUR3.00.00 airfoil outperforms the other two airfoils. The smoothing of the lower surface has allowed attached laminar flow on the airfoil for a wider range of angle of attacks.

Perhaps a better test of the optimized airfoils is the E420 airfoil designed by Eppler.[14] This modern airfoil is also designed for high lift using a different approach than the one taken here and has a thickness of 14.08%. Figure 4 shows a comparison of the lift curves of the E420 and OPTM.TUR3.00.00 airfoils at a Reynolds number of 3×10^6. It can be seen that the Eppler airfoil has about a 30% higher maximum lift coefficient at $\alpha = 10$ deg. Therefore, the optimized airfoil produces high lift, but not the maximum lift possible under all design conditions. In fact, Eppler[14] argues that an optimized airfoil based on Liebeck's ideas is not optimum. However, this does not mean that the Eppler airfoil is superior to the OPTM.TUR3.00.00 airfoil. Figure 5 shows that the optimized airfoil still provides a much better lift-to-drag ratio than the Eppler airfoil. The Eppler airfoil is designed for maximum at the sacrifice of all other performance characteristics. It is also a highly cambered airfoil with an unusual shape that may not be practical in all applications. Furthermore, it is not explained in Ref. 14 exactly how the E420 airfoil was found. Therefore, we believe that Liebeck's optimization procedure

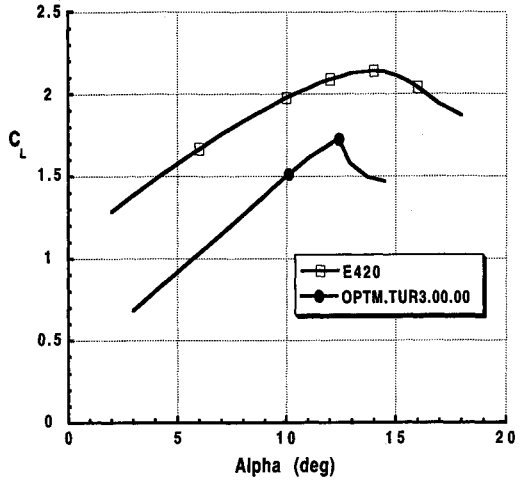

Fig. 4 Lift curves of the Eppler 420 and OPTM.TUR3.00.00 airfoils.

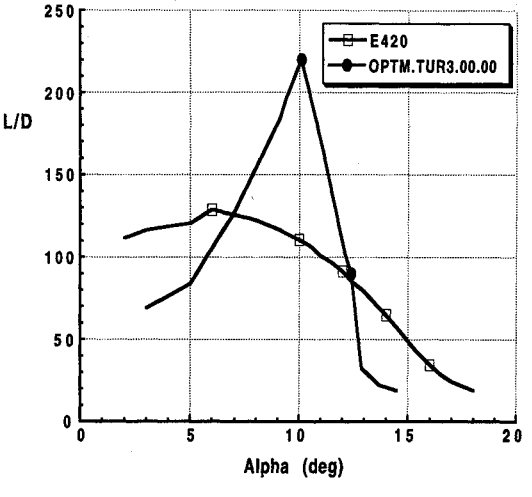

Fig. 5 Lift-to-drag ratios of the Eppler 420 and OPTM.TUR3.00.00 airfoils.

can still be used as a starting point for the design of practical high-lift airfoils.

III. Modified Stratford Distribution

While the above airfoils show good lift and lift-to-drag characteristics, their abrupt stall makes them impractical for applications where the angle of attack nears the stall angle. This is due to the tendency of the Stratford recovery region to separate simultaneously over the entire recovery region. This happens as the skin friction along this region is identically zero. Once the trailing edge of the airfoil separates, the remainder of the recovery region will also detach at that same angle of attack. This leads to a very sudden and dramatic stall which can make these airfoils impractical for general aviation use.

In order to alleviate this problem a modified Stratford distribution was developed. The slope of the original Stratford distribution is modified to allow for a finite skin friction value at the beginning of the recovery region, x_0. The form of the modified distribution is such that the skin friction will decrease linearly to a value of 0 at the trailing edge. *PR* is introduced to control the amount of skin friction at the location x_0. *PR* thus represents the ratio of the slope of modified Stratford distribution to the original Stratford distribution at the location x_0.

The original Stratford distribution consists of a constant pressure region for a distance x_0, followed by a turbulent region of pressure recovery that begins at $x = x_0$. $\bar{C}_P$ is defined using rooftop conditions as reference values. A pressure coefficient and Reynolds number are given by

$$\bar{C}_P = \frac{P - P_0}{1/2\rho V_0^2} \qquad Re_{x_0} = \frac{V_0 x_0}{\nu} \tag{1}$$

where P_0 and V_0 are the pressure and velocity along the constant pressure region. Stratford's distribution is then given by

$$\bar{C}_P \leq \frac{n-2}{n+1} \quad \bar{C}_P(x/x_0) = 0.645\left\{0.435 Re_{x_0}^{1/5}\left[\left(\frac{x}{x_0}\right)^{1/5} - 1\right]\right\}^{2/n}$$

$$\bar{C}_P \geq \frac{n-2}{n+1} \quad \bar{C}_P(x/x_0) = \frac{a}{\sqrt{x/x_0 + b}} \tag{2}$$

with the constants a and b chosen to match $\bar{C}_P$ and its derivative when $\bar{C}_P = (n-2)/(n+1)$ and $n = \log_{10} Re_\infty$. In these formulas, x is measured along the surface of the airfoil. The Stratford pressure coefficient is related to the freestream pressure coefficient by

$$C_P = \left(\frac{V_0}{V_\infty}\right)^2 (\bar{C}_P - 1) + 1 \tag{3}$$

whereas trailing-edge conditions give

$$\left(\frac{V_0}{V_\infty}\right)^2 = \left(\frac{1 - C_{P_{te}}}{1 - \bar{C}_{P_{te}}}\right) \tag{4}$$

and finally

$$Re_{x_0} = \frac{V_0 x_0}{V_\infty s_1} Re_\infty = \sqrt{\left(\frac{1 - C_{P_{te}}}{1 - \bar{C}_{P_{te}}}\right)} \frac{x_0}{s_1} Re_\infty \tag{5}$$

The modified Stratford distribution for $x_0 \leq \zeta \leq XT$ is then given by

$$\frac{d}{d\zeta}[\bar{C}_{P_M}(\zeta)] = a(\zeta)\frac{d}{d\zeta}[\bar{C}_P(\zeta)]$$
$$a(\zeta) = \frac{1 - PR}{XT - x_0}(\zeta - x_0) + PR \tag{6}$$

Integration of Eq. (1) yields the modified Stratford distribution given by

$$\bar{C}_{P_M}(\zeta) = a(\zeta)\bar{C}_P(\zeta) - a'(\zeta)\int_1^z \bar{C}_P(\varsigma)\, d\varsigma \tag{7}$$

It can be seen that this equation reduces to the original Stratford distribution for $PR = 1.0$.

Thus, for the same rooftop length and trailing-edge pressure coefficient the modified Stratford distribution will recover less overall pressure than the original Stratford distribution, but will be less prone to separation.

The OPT.TUR3.00.XX series of airfoils was developed with this in mind. Figure 6 shows a family of upper surface pressure distributions for these airfoils with varying modified PR. As expected, as PR is increased, the upper surface lift coefficient decreases due to the fact that the maximum lift condition is no longer met.

Figure 7 shows the lift curves of three airfoils with pressure recovery factors of 0.80, 0.90, and 1.00. Surprisingly, OPT.TUR3.00.00 and OPT.TUR3.00.90 have nearly identical lift curves with very sharp drops in lift coefficient around $\alpha = 12$ deg with $C_{L\max} = 1.72$. The OPT.TUR3.00.80 airfoil has a much smoother lift curve with $C_{L\max} = 1.45$ at $\alpha = 8.45$ deg. Thus, the penalty of smoothing the lift curve is a 15% loss in maximum lift coefficient.

It can be seen from Fig. 8 that the modified Stratford airfoils have a spike in the lift-to-drag ratio curve around the design angle of attack just as the original airfoils have. However, the magnitude of the peak of the OPT.TUR3.00.80 is about 15% lower than the unmodified airfoil. The low lift-to-drag ratio of the OPT.TUR3.00.90 could possibly be improved with further optimization of the lower surface. Another effect of the modified Stratford distribution is a lowering of the design angle of attack for the OPT.TUR3.00.80 to 4.2 deg. The modified airfoil also stalls 5 deg past its design angle, at $\alpha = 9$ deg, while the OPT.TUR3.00.00 stalls at only 3 deg above its design angle.

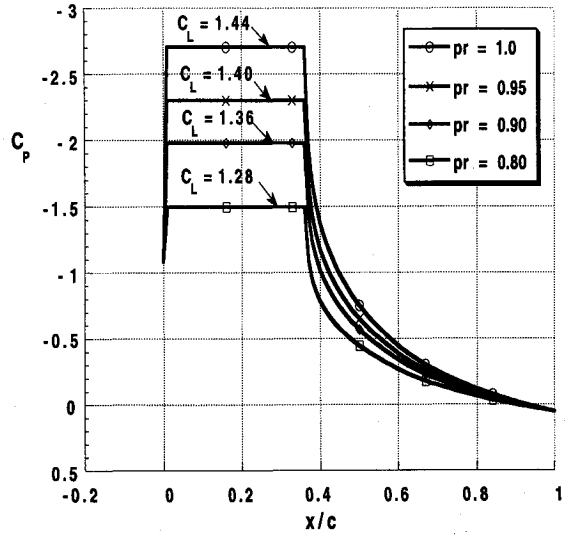

Fig. 6 Family of modified Stratford distributions for $Re = 3 \times 10^6$.

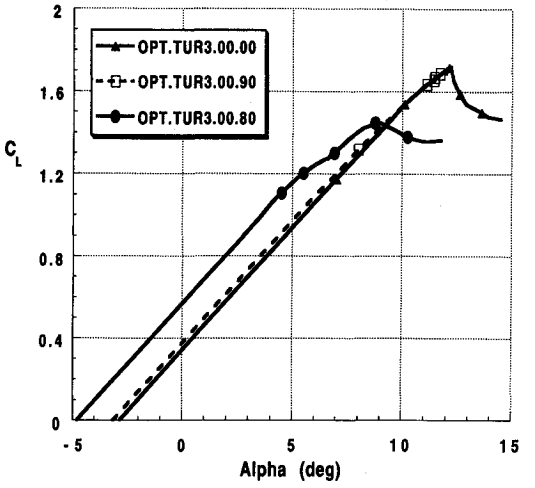

Fig. 7 Lift curves for the OPT.TUR3.00.XX series of airfoils.

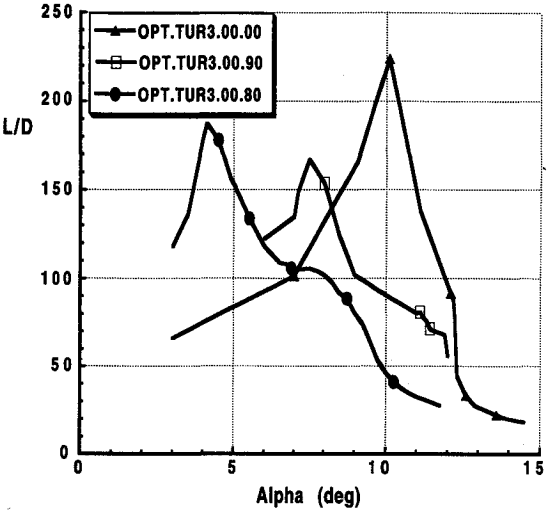

Fig. 8 Lift-to-drag ratios of the OPT.TUR3.00.XX series of airfoils.

IV. Compressible Airfoils

Following the suggestion of Narramore et al.,[6] compressibility effects are accounted for by using isentropic flow relations. C_P is defined as

$$C_P = \frac{2}{\gamma M_\infty^2}\left(\left\{\frac{1 + [(\gamma - 1)/2]M_\infty^2}{1 + [(\gamma - 1)/2]M^2}\right\}^{[\gamma/(\gamma-1)]} - 1\right) \tag{8}$$

C_P can be expressed in terms of the Stratford pressure coefficient:

$$C_P = \frac{2}{\gamma M_\infty^2}\left(\left\{\frac{1 + [(\gamma - 1)/2]M_\infty^2}{1 + [(\gamma - 1)/2]M_o^2}\right\}^{[\gamma/(\gamma-2)]} \times \left(\frac{\gamma}{2}M_\infty^2\bar{C}_P + 1\right) - 1\right) \tag{9}$$

the rooftop velocity by

$$\frac{V_o}{V_\infty} = \left(\frac{1 + 5/M_\infty^2}{1 + 5/M_o^2}\right)^{1/2} \tag{10}$$

and finally

$$\bar{C}_P = (2/\gamma M_\infty^2)\{[1 + \tfrac{1}{2}(\gamma - 1)(1 - V_o^2)M_\infty^2]^{[\gamma/(\gamma-1)]} - 1\} \tag{11}$$

In order to validate the compressible version of OPTIMUM, we attempted to verify the results presented by Narramore et al.[6] A family of optimized upper surface pressure distributions along with upper surface lift coefficients was presented by Narramore for design conditions of $Re = 4 \times 10^5$, $C_{Pte} = 0.1$, $M_\infty = 0.4$, and a fully turbulent rooftop. It was found these curves match those of Narramore (to within the accuracy of determining his results from a published figure) for values of C_{Pminn} and location x/c of the start of the Stratford recovery region.

However, the values of C_{Lu}, the lift coefficient for the upper airfoil surface only, from OPTIMUM were much lower than Narramore's reported values. The curves from OPTIMUM, however, do show the general trend of decreasing lift coefficients with increasing Mach number.

One possible explanation for these differences is that Narramore, although he does not explicitly state so, may have used a linear theory in his optimization procedure. This is suggested by his use of x/c in his paper as the independent variable instead of $s/(s_1 - s_3)$. In order to check this, OPTIMUM was run using a linear theory. This allows the calculation of linear values of C_{Pminn} and C_{Lu}, although the inverse code cannot be run because it requires the nonlinear theory. The output linear lift coefficients, also shown in Fig. 9, still did not match the values reported by Narramore. It should be noted that the linear lift coefficients from OPTIMUM for incompressible flow, $M_\infty = 0$, did match those reported by Liebeck[4] and Smith[1] in their papers. It is interesting that the linear method produces higher lift coefficients for the laminar case and lower lift coefficients for the turbulent case.

When designing compressible airfoils it turns out that the input lower surface velocity distribution must be modified, because the boundary-layer growth changes. In practice this is done by iterating on the modified velocity distributions output by OPTIMUM until a reasonable airfoil is obtained. In practice, as the Mach number increases, the lower surface velocity should have a steeper initial acceleration region than in the incompressible case. The compressible distribution then flattens to a near constant value until a short distance from the trailing edge when a sudden jump occurs to match the trailing-edge velocity.

Figure 10 shows airfoils found for $M_\infty = 0.00$, 0.10, 0.20, 0.30, and 0.40, respectively, and a freestream Reynolds number of 3×10^6. As compared to the incompressible airfoil, the compressible airfoils have their maximum thickness further back, less maximum thickness, and less camber. This is exactly what Narramore reported for his results using an inverse code based on solving the full Navier-Stokes equations.

Drela's code was used to evaluate the performance of the OPT.TUR3.40.00 airfoil at the design conditions. Drela's code

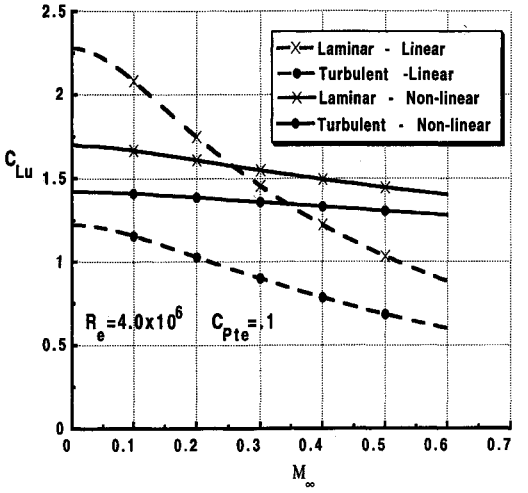

Fig. 9 C_L vs Mach number as generated by OPTIMUM.

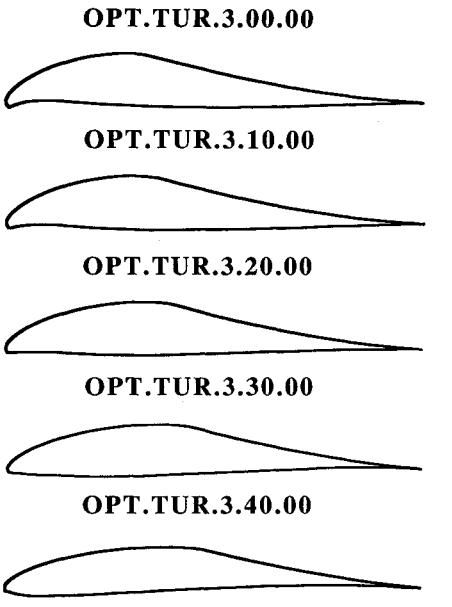

Fig. 10 Series of optimized airfoils designed for varying Mach numbers.

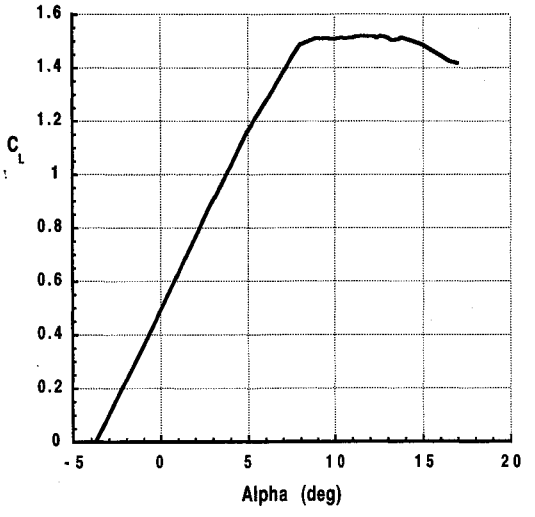

Fig. 11 Lift curve of the OPT.TUR3.40.00.

uses Von Karmen-Tsien relations for pressure coefficient and velocity. Figure 11 shows a surprising lift curve for the OPT.TUR3.40.00 airfoil. The sudden stall characteristic of the incompressible airfoils has been replaced by a large region of constant lift coefficient. Therefore, compressibility effects seem to create a Stratford distribution that stalls smoothly.

As the stall characteristics of an airfoil are due to boundary-layer effect, this similarity in lift curves implies similar boundary-layer behavior. Thus, the form that has been chosen for the modified Stratford distribution in incompressible flow behaves as the original Stratford distribution in compressible flow. This indicates that the compressibility effects that have been made have altered the zero skin friction condition in the Stratford distribution, and are in fact too conservative and maybe Stratford's distribution should be modified for compressible flow. A possibility exists to then gain better performance out of the compressible airfoils.

The lift-to-drag ratio of the compressible airfoil displays the same peak around the design angle of attack as the incompressible airfoils. Again, in a manner similar to the modified Stratford airfoils, the design angle of attack is lower than a comparable incompressible airfoil. Finally, the maximum lift-to-drag ratio, ranging from 220 at $M_\infty = 0.0$ to 235 at $M_\infty = 0.40$, appears to be unaffected by compressibility effects and

is a near constant throughout the range of Mach numbers examined in this study.

V. Drag Optimization

Alternatively, the problem of minimizing drag or maximizing lift-to-drag ratio can be considered. Previously, little research has been done on this subject. In this case only incompressible flow will be considered over the top surface of the airfoil with the bottom surface left free to ensure a practical airfoil shape. Although the drag of the bottom airfoil surface is on the same order as the upper airfoil surface, it is believed that as long as the flow is kept accelerating on the bottom surface, thus avoiding pressure drag, the drag will be kept near its minimum value.

Therefore, to a first approximation, only the upper airfoil surface is optimized using the Squire-Young[15] relation for drag based on the momentum thickness of the boundary layer, which can in turn be related to the potential velocity. This relation is limited to Reynolds numbers between 5×10^5 and 5×10^7, and flows not near separation.

The total boundary-layer drag coefficient is given by

$$C_D = 2\theta_{te}(u_{e_{te}}/u_\infty)^{3.2} \tag{12}$$

where θ_{te} is the momentum thickness at the trailing edge, and u_e is the potential velocity. The momentum thickness is evaluated from

$$\theta^{1.25}u_e^{4.25}\Big|_{x_t}^{x} = 0.963Re^{-0.25}\int_{x_t}^{x} u_e^4\,dx \tag{13}$$

where x_t is taken as the transition point, and θ_{x_t} is given by

$$\theta_{x_t}^2 = 0.45\,\frac{1}{Reu_{e_{xt}}^6}\int_0^{x_t} u_e^5\,dx \tag{14}$$

If $x_t = 0$, the momentum thickness is given by

$$\theta^2 = (0.075/\beta Re) \tag{15}$$

For this case, a more general velocity distribution is used. It is assumed to consist of a rooftop or constant velocity region of length x_0 followed by a recovery region where the velocity is given by

$$V(\zeta) = V_o\left[1 + \frac{(V_{te}/V_o)^{-1/\mu} - 1}{1 - x_0}(\zeta - x_0)\right]^{-\mu} \tag{16}$$

where lengths are taken to be normalized by the chord length. This form is taken from Eppler[14] who developed it for use in his inverse code.

The optimization task is to find the rooftop length, and therefore the height, which optimizes the drag for a given set of flow conditions and recovery parameter μ which controls the steepness and shape of the recovery profile. A value of $\mu \approx 0.21$ represents a Stratford distribution.

The solution to the minimum drag problem was found to be a rooftop distribution over the entire upper surface with no pressure recovery region. Thus, no true minimum exists. This is believed to be due to the dependence of the drag on velocity to the fourth power. The rooftop level must be kept as low as possible, which is done by having little or no pressure recovery. This was found to hold regardless of the choice of μ. μ should then be chosen on the basis of other design considerations where higher μ result in steeper recovery functions and can result in hard stall characteristics.

An airfoil has been optimized for minimum drag at $\mu = 0.21$, with the rooftop length chosen as 90% chord length. This represents about the limiting size of the rooftop for a realistic airfoil shape. This airfoil can then be compared to an airfoil designed for maximum lift. The OPTD.TUR3.00.00 airfoil, shown in Fig. 12, is a 26%-thick airfoil with a large amount of camber near the trailing edge, giving a zero lift moment coefficient of -0.30. The drag curves are given in Fig. 13. At low angles of attack near its design angle of 3.5 deg it has a much lower drag than the OPTM.TUR3.00.00, as predicted. At higher angles of attack the OPTD.TUR3.00.00 has a much higher drag. However, for applications where the angle of attack is fixed and the large moment is acceptable, the OPTD.TUR3.00.00 does show good drag characteristics with lift coefficients ranging from 0.45 at $\alpha = -0.5$ deg to $C_L = 0.95$ at $\alpha = 5.0$ deg.

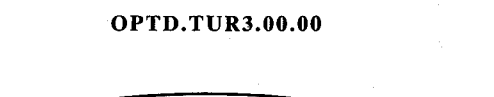

Fig. 12 Airfoil optimized for minimum drag.

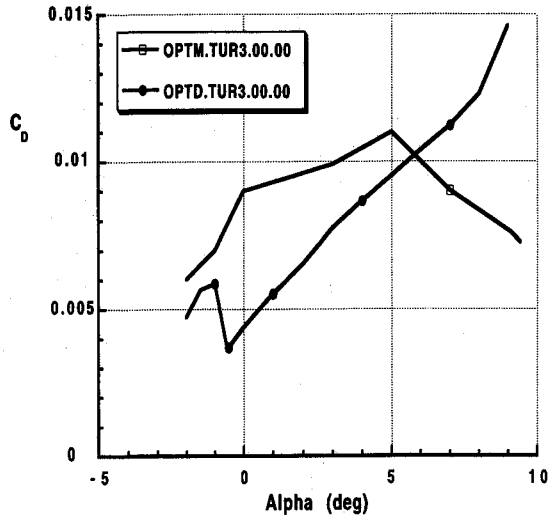

Fig. 13 Comparison of drag coefficients for optimized airfoils designed for low drag and high lift.

The lift-to-drag ratio of the OPTD.TUR3.00.00, although lower than that of the OPTM.TUR3.00.00, is still quite good over the design range. The maximum lift-to-drag ratio of 125 occurs near zero angle of attack and then remains above 100 up to $\alpha = 8$ deg.

The effect of μ on the values of C_L, C_D, and L/D has also been studied. It has been found that C_L increases linearly with μ, C_D decreases quadratically with μ, and therefore, L/D increases in a cubic manner with μ. This supports the view that the Stratford distribution, which is approximated by $\mu = 0.21$, is not the ideal recovery region pressure distribution. However, increasing μ also increases the onset of hard stall in these airfoils. Therefore, as μ is increased above 0.21, the airfoil will display even worse stall characteristics than the Stratford-type airfoils. A practical limit is found to be about $\mu = 0.31$, and the designer must make a tradeoff between high lift and hard stall.

VI. Design Example

In many applications the thickness of the airfoil is fixed by structural or internal volume requirements. In this case it is desirable to optimize the performance for a specified thickness. In this design method the airfoil thickness can be related to the rooftop length. This relation is shown in Fig. 14. The optimization procedure is then constrained to a user specified rooftop length. This relation is not exact as the modification of the lower surface may lead to small changes in the thick-

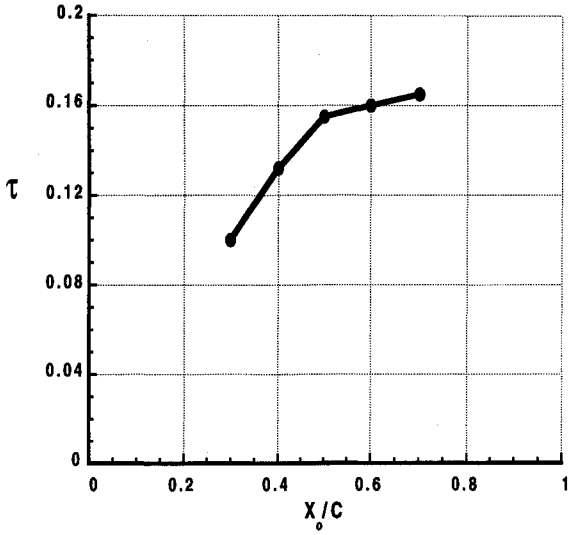

Fig. 14 Relationship between rooftop length and airfoil thickness ratio.

WIND.1

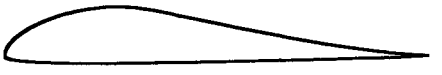

Fig. 15 WIND.1 airfoil designed for wind turbine application.

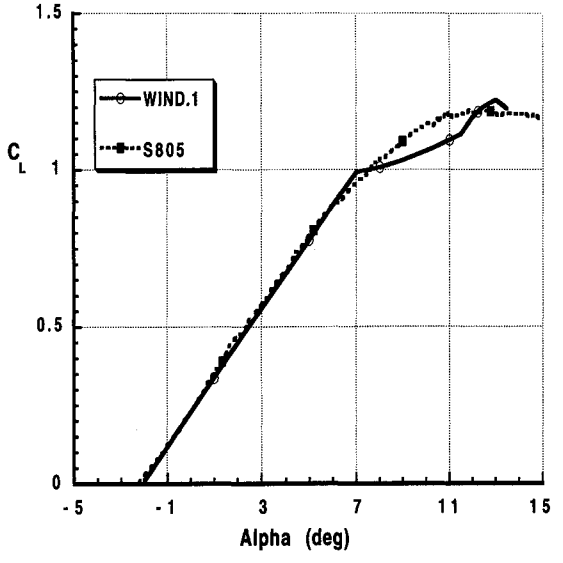

Fig. 16 Lift curve comparison of the WIND.1 and S805 airfoils.

ness, and so it is necessary to iterate the rooftop length until the desired thickness is reached.

Using this procedure an airfoil was designed for a wind turbine application. The airfoil is based on the S805 airfoil developed by Tangler[10] using the Eppler design and analysis code for use on a wind turbine blade. The S805 is designed for a Reynolds number of 2×10^6 with a thickness of 13.5%. Further requirements include a $C_{L\max} \leq 1.29$ in order to limit structural loads, $C_{D\min n} \leq 0.005$, and a $C_{M0} \leq -0.05$.

In an attempt to develop an airfoil that meets all of the above requirements the OPTIMUM code was used to generate the velocity distribution of the WIND.1 airfoil based on an OPTM.LAM2.00.80 airfoil. This velocity distribution was then fine tuned in the Eppler code so that the resulting airfoil had a $C_{L\max} = 1.29$, $C_{D\min n} = 0.005$, and a $C_{M0} = -0.01$.

The resulting airfoil, shown in Fig. 15, was then tested and compared to the results of wind-tunnel tests for the S805 at

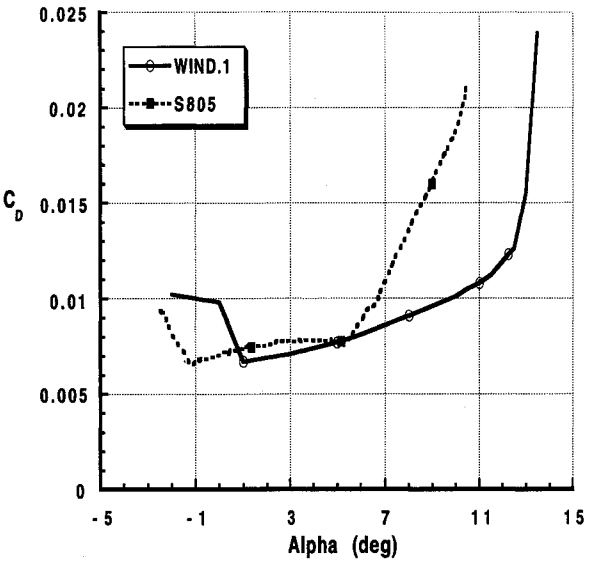

Fig. 17 Drag curve comparison of the WIND.1 and S805 airfoils.

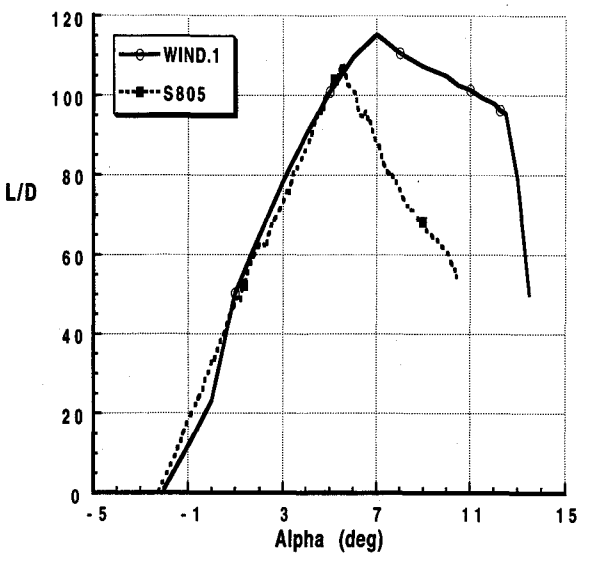

Fig. 18 Lift-to-drag ratio comparison of WIND.1 and S805 airfoils.

a Reynolds number of 1×10^6 given by Tangler.[10] These experimental results were shown to match well with the results predicted by the Eppler code.[10] (A comparison with experimental results was necessary since the coordinates of S805 are not available.) A Reynolds number of 1×10^6, rather than 2×10^6, is chosen for comparison because good drag characteristics are much harder to achieve at lower Reynolds numbers due to the appearance of laminar separation bubbles.

These results are shown in Figs. 16–18. The lift curves are almost identical up to $\alpha = 7$ deg where the WIND.1 airfoil experiences a dip in relation to the S805. The drag of the WIND.1 is lower than that of the S805 over most angles of attack, whereas the lift-to-drag ratio of the WIND.1 is similar to the S805 up to about 6 deg, and then becomes much higher. The results for $Re = 2 \times 10^6$ are very similar with the WIND.1, having lower drag over most angles of attack and a higher lift-to-drag ratio at high angles of attack. The major difference in these two cases is that the dip in the lift curve of the WIND.1 disappears at the higher Reynolds number. It thus appears that a small laminar separation appears on the upper surface of the airfoil at low Reynolds numbers. It is believed that further refinement of the WIND.1 airfoil will improve its performance by removing the laminar separation bubble at low angles of attack and the dip in the lift curve at high angles of attack. It should be noted that S805 was designed to be

insensitive to surface roughness. We believe that WIND.1 is also insensitive to surface roughness, but some experimental work needs to be done for a fair comparison of the two airfoils.

VII. Conclusions

A method of designing optimized airfoils for maximum lift in subcritical flow based on Liebeck's nonlinear method is presented. Airfoils are designed which provide higher lift and better lift-to-drag ratios than conventional airfoils. A modified Stratford distribution has also been developed which reduces the abrupt stall typical of this class of high-lift airfoils.

Optimization for minimum drag is also done by expressing the drag coefficient in incompressible flow on the potential velocity. Preliminary results show that these airfoils display low drag near their design angles of attack.

As one specific example of this method the preliminary design of the WIND.1 airfoil was found not only to meet all the design requirements of the S805 airfoil developed by Tangler, but to also result in higher lift-to-drag ratios at high angles of attack. In both cases Eppler's code was used, but the WIND.1 airfoil was optimized using Liebeck's method. Therefore, it is believed that Liebeck's method coupled with Eppler's code can be used to develop optimized airfoils for a wide range of applications.

Future extensions to this work include the development of a compressible form of the drag optimization and a better method of controlling the airfoil thickness.

Acknowledgments

The authors would like to thank the Minnesota Supercomputer Institute (MSI) for supporting this research as well as providing computing facilities and technical support for the calculations done in this study. The authors also wish to thank Mark Drela at MIT, Cambridge, Massachusetts, for providing his airfoil analysis code.

References

[1]Smith, A. M. O., "High-Lift Aerodynamics," Wright Brothers Lecture, AIAA Paper 74-939, Aug. 1974.

[2]Liebeck, R. H., and Ormsbee, A. L., "Optimization of Airfoils for Maximum Lift," *Journal of Aircraft*, Vol. 7, No. 5, 1970, pp. 409–415.

[3]Liebeck, R. H., "A Class of Airfoils Designed for High Lift in Incompressible Flow," *Journal of Aircraft*, Vol. 10, No. 10, 1973, pp. 610–617.

[4]Liebeck, R. H., "Design of Subsonic Airfoils for High Lift," *Journal of Aircraft*, Vol. 15, No. 9, 1978, pp. 547–561.

[5]Lyrintzis, A. S., Bergeles, G., and Athanassiadis, N., "Optimized Airfoils for Wind Energy Applications," *Proceedings of the European Wind Energy Association Workshop on Wind Energy Applications*, Delphi, Greece, pp. 170–177.

[6]Narramore, J. C., Malone, J. B., and Vermeland R., "Application of a New Navier-Stokes Inverse Method to the Design of Advanced Airfoils," *Proceedings of the American Helicopter Society 46th Annual Forum*, Vol. II (Washington, DC), edited by G. Bengeles, and J. Chadjvaliadis, Atelier-Montage-Printing, Athens, Greece, May 1990, pp. 1089–1098.

[7]Volpe, G., "The Inverse Design of Closed Airfoils in Transonic Flow," AIAA Paper 83-0504, Jan. 1983.

[8]Lyrintzis, A. S., and Farmer, J. D., "On the Design for Maximum Lift Airfoils," *Multidisciplinary Applications of CFD*, Vol. 129, American Society of Mechanical Engineers Winter Annual Meeting, Atlanta, GA, Dec. 1991, pp. 63–74.

[9]Strand, T., "Exact Method of Designing Airfoils with Given Velocity Distribution in Incompressible Flow," *Journal of Aircraft*, Vol. 10, No. 11, 1973, pp. 651–659.

[10]Tangler, J. L., "Status of the Special Purpose Airfoil Families," Windpower '87 Conf., Solar Energy Research Inst. Rept. TP-217-3264, San Francisco, CA, Oct. 1987.

[11]Drela, M., and Giles, M. B., "Viscous-Inviscid Analysis of Transonic and Low Reynolds Number Airfoils," *Journal of Aircraft*, Vol. 25, No. 10, 1988, pp. 1347–1355.

[12]Stratford, B. S., "The Prediction of Separation of the Turbulent Boundary Layer," *Journal of Fluid Mechanics*, Vol. 5, Pt. 1, 1959, pp. 1–16.

[13]Lighthill, M. J., "A New Method of Two-Dimensional Aerodynamic Design," British Aeronautical Research Council, R&M 2112, London 1945.

[14]Eppler, R., *Airfoil Design and Data*, Springer-Verlag, New York, 1990.

[15]Young, A. D., *Boundary Layers*, edited by J. S. Przemieniecki, AIAA Education Series, AIAA, Washington, DC, 1989.